Synthesis and characterization of silica-chitosan hybrid materials as antibacterial coatings for dental implants

B.Palla[1], M. Gurruchaga[1] *, N. Araújo-Gomes[2], M.Fernández[3], L.Rojo[3], J.Suay[2], I. Goñi[1]

[1]: *Department of Science and Technology of Polymers, POLYMAT (Institute of Polymeric Materials), Faculty of Chemistry, University of the Basque Country (UPV/EHU), Pº Manuel de Lardizabal, 3. 20018-San Sebastián, Spain*

[2]: *Department of Industrial Systems Engineering and Design. Universitat Jaume I, Av. Vicent-Sos Baynat s/n. 12071-Castellón, Spain.*

[3]: *Institute of Polymer Science and Technology, CSIC and CIBER-BBN, c/Juan de la Cierva 3, 28006-Madrid, Spain*

ABSTRACT

Although implants are becoming increasingly common in dental practice, before implantation strict patient selection criteria have to be implemented since the implants should have a good chance of osseointegration into the maxillary bone. Moreover, the implanted sites can become severely infected and, consequently, the implant might have to be removed. To avoid implant-related infections and to promote the osseointegration of commercial Titanium implants, different silica-chitosan matrices were synthesized using the sol-gel process. Three different alkoxysilanes were used, methyltrimethoxysilane (MTMOS), 3-glycidoxypropyltrimethoxysilane (GPTMS), and tetraethoxysilane (TEOS). The network formed during the matrix synthesis gradually degrades in aqueous media, and during this hydrolytic degradation, silicon is released, inducing bone formation. Chitosan, with its high biocompatibility and strong antibacterial activity, was selected to confer antibacterial properties to the coatings. The synthesized hybrids were characterized using ^{29}Si- and ^{13}C-NMR to verify the correct formation of the network. The technique was also used to confirm the covalent union between chitosan and the silicon network. Hydrolytic degradation and silicon release studies in the aqueous media were examined, showing the effective silicon release from the hybrids. The analysis of cell cultures *in vitro* demonstrated that the hybrid coatings were not cytotoxic and promoted cell proliferation on their surfaces. The coatings containing 5%–10% chitosan had substantial antibacterial properties. The introduction of different amounts of chitosan and TEOS modulated the degradation of the coatings and, consequently, the Si release.

INTRODUCTION

In the last decades, the number of oral implantations has increased dramatically[1] and now Ti dental implants are widely used. This material has excellent properties, including high biocompatibility, lack of cytotoxicity, and very good anticorrosion and mechanical characteristics in comparison with the natural tooth tissues[2].

The Ti implants are known for their excellent survival record, successful replacement of missing tooth functions, and aesthetic quality[3, 4, 5, 6]. However, strict patient selection criteria have to be followed to assure good osseointegration[7] into the maxillary bone. To overcome this problem, titanium surfaces with new characteristics are being developed. The aim is to obtain surface composition and topography to enhance cell–surface interactions accelerating the osseointegration process, thus ensuring the success of implantation[8, 9].

Another serious problem associated with implantations is the risk of developing infections, such as peri-implantitis[3, 10], caused by bacterial colonization. Such infections might lead to surgical removal of the implant to avoid inflammatory reaction with consequent loss of supporting bone around the implant. The oral cavity is a favorable environment for the development of bacterial biofilms and the subsequent infections due to the accumulation of bacteria. In all cases, bacterial biofilm formation follows a specific pattern that starts with an initial fast colonization followed by a slower, second interbacterial colonization[11, 12, 13]. After the implantation, the bacteria migrate from small spaces in the oral tissues to the implant surface and the implant site. This phenomenon can be observed from the very moment of

implant insertion[14]. Once a biofilm is formed, it is very difficult to eliminate because of the resistance of the bacteria to conventional antibiotic therapies.

The development of antibacterial implant surfaces preventing adhesion and colonization of bacteria is a promising strategy in the fight against infections. The research in this field has become very active; different antibacterial implants are made employing physicochemical modifications of implant surface properties such as roughness, hydrophilicity and surface energy[14, 15] or using different antibacterial molecules (metals, metallic nanoparticles, antibiotics, cationic compounds, etc.[16, 17, 18]).

These antibacterial strategies can be categorized into two basic types, attempting to prevent bacterial adhesion or trying to eradicate already formed biofilms. A successful prevention might reduce bacterial colonization and the subsequent biofilm formation but, once a biofilm is formed, this method cannot eliminate it. The materials that eradicate biofilms deliver a burst release of an antibacterial agent but in the long-term leave the site open to a further infection.

In view of the available information, the aim of this work was to obtain new active surfaces for dental implants. Such surfaces should have not only good osseointegration properties but also a strong antibacterial activity over prolonged periods, either blocking the initial bacterial adhesion or preventing later infections.

To achieve this, chitosan was used as the antibacterial agent. In the past few years, chitosan has been widely investigated in biomaterial research projects. Some of its outstanding characteristics are high biocompatibility, biodegradability, and hydrophilicity; it is also non-toxic[19, 20, 21, 22]. Chitosan has strong antibacterial properties[23]. The antimicrobial activity of this compound is associated with the positively charged amino groups of its structure; they interact with the negatively charged bacterial cell wall, killing the bacteria[24, 25]. Nowadays, one of the most common strategies is the synthesis of chitosan nanoparticles because of their large surface area and high affinity to bacterial cells. These particles exert a quantum size effect, leading to the disruption of the membrane and to a stronger antibacterial activity[26]. They can also act as drug carriers for other antibacterial molecules [24, 27, 28, 29]. However, most commonly, chitosan is used directly in a coating to protect the surface. Under such conditions, it acts as a bacteriostatic agent preventing bacterial adhesion[30]. Its antibacterial effect is enhanced in combination with other antibacterial molecules, such as antibiotics. This has been shown in the case of chitosan-vancomycin coatings, where it serves as a matrix for the encapsulation and release of vancomycin[28, 29]. However, chitosan and chitosan-based coatings have relatively low stiffness and strength, especially in moist environments. Several researchers have obtained modified chitosan preparations to improve its mechanical properties; one of the most important modifications has been achieved using the sol-gel method[31, 32].

As we have demonstrated in our previous papers[9, 33], the sol-gel method is a relatively simple and inexpensive way to synthesize different coatings that can be applied directly to the implant surface, conferring the desired osteoinductive and antibacterial properties. The most commonly used precursors are Si-alkoxides. The final materials obtained using these

precursors are biocompatible and bioresorbable *in vivo*. They release Si compounds with osteoinductive properties, which promote the activity of bone-forming cells[34] and protect the implant against corrosion[35, 36, 8]. This behavior seems to improve bone regeneration ability of these coatings *in vivo*, accelerating the formation of new bone spicules[9]. Moreover, studies of foreign body response parameters have proven the biocompatibility of these materials, confirming their suitability for dental implant applications.

The assumption of the current study was that it should be possible to obtain a coating that prevents the long-term bacterial adhesion and has osteoregenerative properties. To this end, chitosan was included in coatings obtained using the sol-gel method.

The sol-gel coatings were designed on the basis of two alkoxysilane precursors, MTMOS and GPTMS, used in different molar ratios. The MTMOS precursor should provide a high biocompatibility and low biodegradability. The GPTMS allows functionalization through the epoxy ring of its structure, with the covalent bonding between this oxirane group and the amino groups of chitosan, as it has been found in previous studies[23, 37]. In addition, Shirosaki *et al*. have found that chitosan-GPTMS hybrids show better biocompatibility than chitosan itself. These hybrids also have excellent cytocompatibility and allow the proliferation of MG63 osteoblastic cells and human bone marrow cells[38, 39].

Moreover, the orthosilicic acid released by these coatings has an osteoinductive effect enhancing the formation of bone tissue[37]. One of the objectives of this work was to promote the formation of bone around the implant, or at least not to hinder the process of osseointegration. For that purpose, a small amount of tetraethyl orthosilicate (TEOS) was also added to the formulation, to modulate the degradation rates.

To summarize, we prepared various formulations of sol-gel hybrids doped with different amounts of chitosan. We examined the effect of their composition on various important properties, such as the hydrolytic degradation and silicon release from the coatings. We also assessed their impact on bacterial growth *in vitro*.

MATERIALS AND METHODS

MATERIALS

Different Si-chitosan hybrid coatings were synthesized using the sol-gel method, with 0.1 N HCl as a catalyst. These formulations were composed of three different alkoxysilanes: MTMOS, GPTMS, and TEOS, all purchased from Sigma-Aldrich (St. Louis, MO, US) and used without further purification. Chitosan of 75%–85% degree of deacetylation (Sigma-Aldrich) was used as the antibacterial agent.

SYNTHESIS

The initial solution contained the different silicon precursors with 2-propanol (Sigma-Aldrich). The volume ratio of alcohol to precursor was 1:1. The solution was stirred on a magnetic plate, and a stoichiometric amount of catalyst was added (water acidified with

hydrochloric acid to obtain pH 1). To carry out the hydrolysis and condensation reactions, the mixture was kept under stirring for 1 h to ensure the homogeneity of the sol. Then, the mix was left at room temperature for another hour before its deposition on the substrates.

For chitosan-containing formulations, chitosan was first dissolved in 2% acetic acid (Sigma-Aldrich). Afterward, the corresponding amount of GPTMS was added, and the reaction was allowed to proceed for 2 h. This step was included to promote a prehydrolysis stage, favoring the formation of covalent bonds between the two structures[38, 39]. Then, the sol-gel synthesis using the remaining alkoxysilane precursors was carried out in 2-propanol (Sigma-Aldrich). A stoichiometric amount of hydrochloric acid (0.1 N HCl) (Panreac, Barcelona, Spain), the catalyst, was added drop by drop, and the mixture was left to react for 1 h. Then, the two reaction mixtures were pooled and allowed to react for 90 min at room temperature. Finally, the gels were applied onto different substrates, depending on the assay, and subjected to heat treatment (100 ˚C, 2 h).

We synthesized two types of coatings, binary materials with two alkoxysilanes (50M50G) and ternary materials with three alkoxysilanes (45M45G10T). The content of chitosan in these materials varied from 0% to 10% (wt/wt) of the precursor weight. The compositions of these formulations are shown in Table 1.

CHARACTERIZATION

Chemical characterization

a) Liquid-state ^{29}Si Nuclear Magnetic Resonance Spectrometry (^{29}Si-NMR)

Liquid-state ^{29}Si-NMR was used to follow the hydrolysis and condensation reactions of the sol-gel process. The spectra were examined at 79.47 MHz and 99.362 MHz, using an FT-NMR Bruker Avance 400 and DPX-500 spectrometers, respectively. A pulse sequence of 5 ms with T_2 filter, acquisition time of 1 s, waiting time of 2 s, number of scans of 384, and a spectral width of 17857 Hz were used.

The annotation system described by Lippmaa and coworkers[40] was employed in all cases. In this system, each silicon atom linked to three alkoxy groups is named T (MTMOS and GPTMS) and the silicon atoms linked to four alkoxy groups, Q (TEOS). The subscript shows the number of oxygens bound to two silicon atoms. Thus, the higher the subscript of the formed species, the greater is the proportion of species with a high degree of condensation, which enhances the formation of a crosslinking structure.

b) Solid-state ^{29}Si Nuclear Magnetic Resonance Spectrometry (^{29}Si-NMR).

Solid-state ^{29}Si-NMR spectroscopy analysis was performed using a Bruker Avance III Spectrometer, model 400 WB Plus, 9.4 (400 MHz), equipped with a Cross Polarization Magic Angle Spinning (CP-MAS) probe. The powdered samples were placed in a 4-mm rotor. ^{29}Si CP-MAS measurements were made at 10 KHz using a 90° proton pulse of 3.5 µs, 2.0-ms contact time, and 5-ms recycle time. The spectra were collected using a 4-mm CP-MAS probe at 79.5

MHz, time domain of 2 K and a spectral width of 32 kHz. The annotation system was the same as for liquid-state spectra.

c) ^{13}C Nuclear Magnetic Resonance (^{13}C-NMR) Spectrometry

^{13}C-NMR spectra were recorded on a Bruker 400 AVANCE III WB Plus spectrometer 9.40 T (^{1}H = 400 MHz) with CP-MAS (Magic Angle Spinning). ^{13}C CP-MAS measurements were taken at 47 kHz using a 90° proton pulse of 3.5 µs, 1.5-ms contact time, and 5-ms recycle time. The spectra were collected using a 4-mm CP-MAS probe at 100.6 MHz, time domain of 2 K, and a spectral width of 29 kHz.

c) Contact angle measurements

The wettability of the hybrid materials was determined by measuring the contact angle using an automatic contact goniometer DataPhysics OCA 20. A sessile drop of 10 µL of deionized water was deposited on a sol-gel coated steel plate at room temperature. Final values are the average of 10 replicates obtained at different spots of three identically prepared samples.

Degradability study

a) Hydrolytic degradation

The hydrolytic degradation test was performed after soaking the coatings (deposited on a glass substrate) in distilled water at 37 °C for 2 months (63 days). The degradation kinetics was evaluated by examining the weight of the coatings before and after soaking for different periods of time. After soaking, the samples were dried in a vacuum oven at 37 °C for 24 h and then weighed. Each data point is an average of three individual measurements.

b) Silicon release test

The quantification of the Si release was performed using Inductively Coupled Plasma Mass Spectrometry (ICP-MS) (Agilent 7700 Series ICP-MS system, Agilent Technologies, USA). Samples were immersed in 50 mL of ultrapure water (MiliQ water) and kept for 2 months at 37 ˚C. For each time point, an aliquot of 50 µL was removed for measurement; the final amount of released Si was expressed in ppm. The cumulative Si release value was obtained from a standard curve obtained using various dilutions of an Si standard (Alfa Aesar, Germany).

***In vitro* assays**

All the materials were sterilized prior to cell culture by exposure to UV radiation for 30 min. *In vitro* MTT-based cytotoxicity assay and cell viability (alamarBlue) assay were carried out. In both cases, human fibroblasts HFB (human epidermal fibroblasts, INNOPROT, Leioa, Bizkaia) were used.

For the MTT assay, the ISO10993-5 standard for biological evaluation of biomedical devices was followed. The coated discs and control Ti discs were incubated at different times

in a 96-well plate (at 37 ˚C). The formazan absorbance was monitored at 570 nm (its quantity presumed to be proportional to the number of viable cells).

To perform the alamarBlue cell viability test, HFBs were cultured for 24 h with the control Ti discs and coated discs, at a density of 60.000 cells/ml, in a 24-well plate. Then, 1 mL of 10% alamarBlue dye (in phenol red-free DMEM) was added to each well and samples were incubated for further 4 h. Aliquots of each sample (100 µL) were transferred to a 96-well plate at chosen time points. The fluorescence emission was measured at 590 nm in a Synergy™ HT Multi-Detection Reader (BioTek Instruments, Winooski, VT, USA). The results were analyzed using one-way analysis of variance (ANOVA), relative to Ti controls. The significance level was set at *$p < 0.05$.

The antibacterial behavior of the tested materials was also examined. In these tests, *Staphylococcus aureus* CECT 86 bacteria were used, following the ISO 22196:2007(E) standard for measurement of antibacterial activity on plastic surfaces. All data were expressed as the mean ± standard deviation. Statistical analyses were performed using ANOVA, employing Origin Software version 8.6 (OriginLab, Northampton, MA, USA). Differences with $p < 0.05$, $p < 0.01$, and $p < 0.001$ were considered statistically significant.

RESULTS

Hybrid sol-gel synthesis and characterization

The progress of hydrolysis and the condensation reactions was studied using liquid-state ^{29}Si-NMR to analyze the behavior of various parameters of the system. Figure 1 shows the degree of condensation reached before the heat treatment of hybrid coatings with and without chitosan. The results were similar for all the formulations; thus, only the spectra of 50M50G and 45M45G10T coatings and the corresponding samples containing 5% of chitosan are shown here.

The introduction of chitosan into the silica materials slows down the reaction, and the hydrolyzed groups of the precursor GPTMS can be found in the network. Nevertheless, the reaction proceeded without hindrance. It resulted in a large number of condensed T_1 species for GPTMS, as well as T_2 species for MTMOS and GPTMS. Moreover, T_3 species were found in the case of 45M45G10T.

To confirm the covalent bonding between chitosan and the silica network via oxirane group of GPTMS[23, 34, 41], solid-state ^{13}C-NMR study was performed. We hypothesized that the epoxy ring would open and react with an amino group of chitosan[42], as illustrated below.

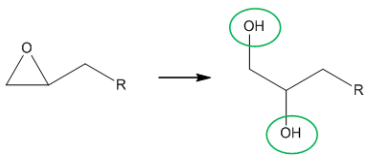

(r.1)

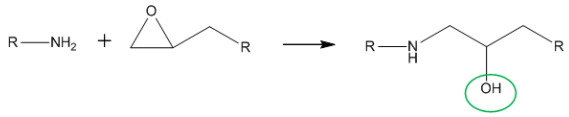

(r.2)

As similar results were obtained for all the formulations, the data for 50M50G with 5% of chitosan are used as an example.

Figure 2 shows the ^{13}C-NMR spectrum obtained for 50M50G hybrid, with the peak assignments[43]. Signal 1 is associated with the non-hydrolyzable methyl group of MTMOS, and the remaining signals correspond to GPTMS. The 50M50G signals from the epoxy ring carbons (peaks 5 and 6) are sharper and more intense than in 50M50G_5%, indicating that in 50M50G, many of the epoxy rings are intact. For the coating with 5 wt% of chitosan, where these peaks are much broader, such differences can be attributed to the opening of the epoxy ring and subsequent reaction with the amino groups of chitosan [23, 34, 41].

Solid-state ^{29}Si-NMR Spectrometry

The final structure of the materials and their degree of condensation after curing was examined using solid-state ^{29}Si-NMR spectroscopy. Figure 3 shows the ^{29}Si-NMR spectra of the 50M50G coatings.

The introduction of chitosan into the silica network affects the crosslinking degree of final materials slightly. For the composition 50M50G, the signals of T_2 and T_3 were observed in all the cases. The T_3 signal was the strongest for most materials, except for 50M50G_10% coating, where the intensity trend of the signals was opposite.

In the case of 45M-45G-10T coatings, apart from the T species from MTMOS and GPTMS, the signals from TEOS (Q species) were also observed for the hybrid without chitosan. In the other cases, these signals were difficult to see because chitosan seems to affect the resolution of the spectra. The behavior of these coatings is similar to those obtained using the 50M50G formulations. When chitosan was added, the siloxane network seemed to be more open as the signal of T_2 was more intense than the T_3 signal. In similarity with 50M50G materials, the 45M-45G-10T coating with 10% (wt/wt) of chitosan formed the most open network, where the signal for the T_2 was stronger than for T_3 species.

The chemical shifts for each species and the peak area ratios for 50M50G and 45M45G10T coatings are summarized in Table 2.

Contact angle measurements

Contact angle values for all the coatings are presented in Figure 4.

The addition of chitosan to the coatings enhanced their hydrophobicity, reflected by an increased contact angle of the hybrids. However, the differences between 50M50G and 45M45G10T materials were not significant.

Hydrolytic degradation

Polysiloxane network degrades in contact with water by hydrolysis, as illustrated by the following reaction[3, 4]: $SiO_2 + H_2O \rightarrow Si(OH)_4$ *(aq.)*

Figure 5 demonstrates the weight loss after different periods of soaking, reflected by the corresponding degradation curves. Degradation kinetics is affected by the composition of the coatings and their chitosan content.

Chitosan increased the degradation rate of the tested materials even though the weight loss was less than 50% over the 2-month period. The 50M50G materials degraded more than 45M45G10T, but their degradation kinetics were slower. The highest levels of degradation were observed for the 50M50G_10% coating.

Silicon release test

Figure 6 shows silicon release from the coatings, measured using ICP-MS, during a period of 2 months.

All the coatings released silicon compounds; a progressive increase in Si release was observed for all the materials during the 2-month assay. In similarity with the degradation results, chitosan increased the amounts of released Si. The 50M50G materials released more Si than 45M45G10T.

***In vitro* assays**

MTT assay

Figures 7a and 7b show the results obtained for the binary and ternary materials.

None of the developed hybrid materials was cytotoxic; all the examined coating samples showed the final cell viability of more than 70% of the viability compared with the control samples (requirement established by ISO 10993-5). In the case of ternary hybrids, the viability was lower than the 70% on the first day of study but increased later, reaching a very high value.

AlamarBlue assay

After testing the cell viability, the ability of HFBs to adhere to and proliferate on siloxane-chitosan coatings was examined.

Figure 8a presents the fluorescence values over time for cells cultured on 50M50G coatings in comparison with the control titanium surfaces. All the materials supported cell proliferation, which increased with the incubation time, especially for the hybrids with 5% and 10% of chitosan.

The 45M45G10T coatings (Figure 8b) showed the same trend as 50M50G materials. After 24 h of incubation, fewer cells adhered to the surface of this coating than to the titanium controls. This trend was reversed after 2 days of culture, resulting in a high final proliferation rate for this coating. The proliferation rates were highest for 45M45G10T and 50M50G materials with 5% and 10% of chitosan.

Twenty-one days after cell seeding, a very extensive cell monolayer was observed on the tested materials, and cellular agglomerates were formed on this monolayer (Figure 9).

Antibacterial activity assay

Finally, the antibacterial activity of the coatings was evaluated by examining the viability of *Staphylococcus aureus* cultured on their surfaces (Figure 10).

The results showed that increasing the percentage of chitosan enhances the antibacterial capacity of the coatings in comparison with titanium controls. The coatings with 5% and 10% of chitosan showed the highest antibacterial activity, particularly marked in the case of ternary hybrids.

DISCUSSION

The long-term performance of the developed silica-chitosan coatings relies on a low degradability of the sol-gel material, retaining the bactericide compound for prolonged periods. This slow degradation process also supplies the orthosilicic acid necessary to promote osteogenesis. Therefore, the examination of the crosslinking degree of the network, its degradation behavior, and the silicon release from the coatings are crucial before the *in vitro* studies can commence

The results of liquid-state ^{29}Si-NMR indicate a considerable effect of chitosan on the condensation process (Figure 1). The comparison of the spectra for the materials with and without chitosan clearly shows that chitosan decreases GPTMS condensation but increases the condensation of MTMOS. Moreover, the addition of TEOS further hinders the condensation of GPTMS. It is possible that the reaction between GPTMS and chitosan through the amino groups, giving rise to large GPTMS/chitosan moieties, creates a steric hindrance in the condensation of the hydrolyzed GPTMS. However, the results of the solid-state NMR study showed (Figures 3a and 3b) that a high degree of crosslinking was achieved for all the materials, with T_2 and T_3 as the dominant structures. During the curing step, chitosan does not disturb the correct formation of the coatings (at least for the chitosan content of up to 10%). Nevertheless, the formed network becomes more open as GPTMS content increases. In the case of 50M50G coatings, the most abundant moiety was the most condensed one, T_3, except for the material with 10% of chitosan, where the T_2 signal was the most intense. This behavior confirms the results obtained during the first part of the condensation reaction. Because of the large size of chitosan molecule and the high viscosity of the reaction mixture, the final structure is more open than the structure obtained using smaller amounts of chitosan. The 45M45G10T formulation showed a similar behavior.

The solid-state ^{13}C-NMR was used to confirm the hypothetical reaction between the epoxy group of GPTMS and the amino group of chitosan[23, 34]. As the recorded spectra demonstrated (Figure 2), no signals were observed at 50 ppm. Such signals would reflect the presence of the methoxy and ethoxy groups of the precursors. Thus, it can be concluded that all the alkoxy groups were successfully hydrolyzed. At 65 ppm, there was a weak signal corresponding to the diol species formed after the opening of the epoxide ring of GPTMS in

acidified water. This signal diminished for chitosan-containing coatings. It is likely that the diol groups disappear after binding with the amino groups of chitosan, as has been shown by IR spectroscopy performed by Shirosaki *et al.*[38], even though other authors report that the diol formation is dominant[37].

Contact angle measurements are essential since the hydrophilic or hydrophobic nature of the material will determine its interactions with the biological environment. We observed (Figure 4) that the introduction of TEOS increased the hydrophobicity of the hybrid coating, reflecting its enhanced crosslinking (see the spectra in Figure 1). However, the presence of chitosan gives rise to coatings with similar contact angle values. Thus, it seems reasonable to assume that once the materials are crosslinked, the organic hydrophobic groups orient themselves toward the surface as a result of the interactions between the chitosan and SiOH. It is very important to note that hydrophilicity is a crucial factor in the cell behavior. All the contact angles measured here were in the range (of 60–80˚) optimal for adequate interactions with the biological environment and the cell attachment[44, 45, 46].

The results of the degradation study tests showed the same trend for all the coatings. Silica-chitosan hybrid coatings had higher degradation rates than the materials without chitosan. This can be attributed to the large size of chitosan molecule, leading to the formation of large bridging bonds, which would reduce the packaging of the network. Such structural changes would favor the uptake of water and, thus, promote the -Si-O-Si- bond hydrolysis[39]. The comparison of materials with and without chitosan revealed the degradation rates of the same order, and none of the hybrids degraded by more than 50% over 2 months. However, during this period, the 45M45G10T materials lost less weight than the binary coatings. These results seem to disagree with the study of Romero-Gavilán *et al*.[47], in which the introduction of TEOS into hybrid materials has increased the hydrolytic degradation. This discrepancy can be attributed to the differences between the heat treatment methods used during the curing stage. In our study, the binary and ternary materials underwent the same heat treatment of 2 hours at 100˚C. However, in the study mentioned above[47], different heat treatment was used for each of the hybrids, i.e. 140 ˚C for 50M50G and 100 ˚C for 45M45G10T. Under such conditions, the crosslinked network formed in the ternary coatings would be more open, favoring the water uptake and the consequent hydrolytic degradation. In contrast, in our study, since the TEOS molecule is smaller and has one more bonding possibility than MTMOS or GPTMS, tight cross-links would be formed under the same curing conditions, hindering the water uptake and, hence, reducing the hydrolysis rate.

To assess the rate of hydrolytic degradation, silicon release was examined. The results revealed the Si release profiles similar to mass loss profiles, as had been expected. Clearly, the 50M50G hybrid released more silicon that the ternary hybrid. This behavior, again, does not agree with the results of other studies. Shirosaki *et al*.[38] have stated that the introduction of TEOS increases the silicon release from chitosan-GPTMS coatings. However, the presence of other alkoxysilanes, such as MTMOS, also affects the network formation. Therefore, as stated before, the addition of TEOS results in a tighter network, reducing the rate of hydrolysis, and thus the silicon release.

The results of *in vitro* tests showed that all the tested materials were non-cytotoxic. This is an important point considering that these materials are going to be in a direct contact with human tissues. Moreover, alamarBlue assay (Figure 9), designed to quantitate the proliferation of different types of cells on the coating surfaces, showed that, for all of the formulations, the cells proliferated well over the tested periods, irrespective of the initial adhesion rate[49, 50, 51]. The rates of proliferation increased with the increasing content of chitosan. Interestingly, HFBs not only grew to confluency but also formed multilayered colonies, demonstrating good biocompatibility of the coatings.

The assessment of the antibacterial activity of the developed materials was the main goal of this work. We found that the antibacterial activity increased with the increasing content of chitosan. This behavior was most pronounced for the hybrids with 5% and 10% of chitosan. This might be associated with the known antimicrobial activity of chitosan, which seems to be more bacteriostatic that bactericidal[21, 24, 27], preventing the bacterial growth on the surfaces in which it is included[30]. The comparison of the hybrid materials showed that 45M45G10T coatings have stronger antibacterial activity than 50M50G. This agrees with the results of the hydrolytic degradation studies, where 50M50G showed a larger mass loss, which might have reduced its antibacterial capability.

CONCLUSION

The addition of chitosan improved the antibacterial activity of the two tested types of silica-chitosan hybrid coatings (50M50G and 45M45G10T), and increased the proliferation rates of the cells grown on their surfaces. The proliferation rates were the highest for the coatings with 5 and 10% of chitosan. We can also conclude that the addition of chitosan and TEOS modulates the Si release, which plays an important role in osteocompatibility. The ternary coatings with 5 and 10% of chitosan have particularly good bactericidal properties. They should be suitable for dental implants as they might confer the protection against bone infection over prolonged periods. The introduction of these materials into the dental practice might increase the number of patients accepted for implantation.

Acknowledgements. This research was supported by the Spanish Ministry of Economy and Competitiveness project MAT2014-51918-C2-2-R, the University of the Basque Country (UPV/EHU) project UFI11/56, Basque Government project IT611-13, and a personal grant (predoc-2016-1-0141). The authors thank for technical and personnel support provided by SGIker of UPV/EHU and the European funding sources (ERDF and ESF). We are especially grateful to Antonio Coso and the personnel of his company (Ilerimplant S.L) for their cooperation.

REFERENCES

1. Subramani, K., & Ahmed, W. (2011). *Emerging nanotechnologies in dentistry: Processes, materials and applications*. William Andrew.

2. Albrektsson, T., Brånemark, P. I., Hansson, H. A., & Lindström, J. (1981). Osseointegrated titanium implants: requirements for ensuring a long-lasting, direct bone-to-implant anchorage in man. *Acta Orthopaedica*, *52*(2), 155-170.

3. Tey, V. H., Phillips, R., & Tan, K. (2016). Five-year retrospective study on success, survival and incidence of complications of single crowns supported by dental implants. *Clinical Oral Implants Research*.

4. Gristina, A. G. (1987). Biomaterial-centered infection: microbial adhesion versus tissue integration. *Science*, *237*(4822), 1588-1595.

5. Atieh, M. A., Alsabeeha, N. H., Faggion Jr, C. M., & Duncan, W. J. (2013). The frequency of peri-implant diseases: a systematic review and meta-analysis.*Journal of periodontology*, *84*(11), 1586-1598.

6. Mombelli, A., & Décaillet, F. (2011). The characteristics of biofilms in peri-implant disease. *Journal of clinical periodontology*, *38*(s11), 203-213.

7. Pye, A. D., Lockhart, D. E. A., Dawson, M. P., Murray, C. A., & Smith, A. J. (2009). A review of dental implants and infection. *Journal of Hospital infection*,*72*(2), 104-110.

8. Le Guéhennec, L., Soueidan, A., Layrolle, P., & Amouriq, Y. (2007). Surface treatments of titanium dental implants for rapid osseointegration. *Dental materials*, *23*(7), 844-854.

9. Martínez-Ibáñez, M., Juan-Díaz, M. J., Lara-Saez, I., Coso, A., Franco, J., Gurruchaga, M., & Goñi, I. (2016). Biological characterization of a new silicon based coating developed for dental implants. *Journal of Materials Science: Materials in Medicine*, *27*(4), 1-9.

10. Grischke, J., Eberhard, J., & Stiesch, M. (2016). Antimicrobial dental implant functionalization strategies—A systematic review. *Dental Materials Journal*,*35*(4), 545-558.

11. Rosan, B., & Lamont, R. J. (2000). Dental plaque formation. *Microbes and infection*, *2*(13), 1599-1607.

12. Ivanova, E. P., & Crawford, R. J. (2015). *Antibacterial Surfaces*. Springer.

13. Godoy-Gallardo, M., Wang, Z., Shen, Y., Manero, J. M., Gil, F. J., Rodriguez, D., & Haapasalo, M. (2015). Antibacterial Coatings on Titanium Surfaces: A Comparison Study Between in Vitro Single-Species and Multispecies Biofilm. *ACS applied materials & interfaces*, *7*(10), 5992-6001.

14. Katsikogianni, M., & Missirlis, Y. F. (2004). Concise review of mechanisms of bacterial adhesion to biomaterials and of techniques used in estimating bacteriamaterial interactions. *Eur Cell Mater*, *8*(3).

15. Renvert, S., & Quirynen, M. (2015). Risk indicators for peri-implantitis. A narrative review. *Clinical oral implants research*, *26*(S11), 15-44.

16. Cloutier, M., Mantovani, D., & Rosei, F. (2015). Antibacterial Coatings: Challenges, Perspectives, and Opportunities. *Trends in Biotechnology*, *33*(11), 637- 652.

17. Hetrick, E. M., & Schoenfisch, M. H. (2006). Reducing implant-related infections: active release strategies. *Chemical Society Reviews*, *35*(9), 780-789.

18. Ferraris, S., & Spriano, S. (2015). Antibacterial titanium surfaces for medical implants. *Materials Science and Engineering: C*.

19. Hasirci, N., & Hasirci, V. (Eds.). (2010). *Biomaterials: From Molecules to Engineered Tissue* (Vol. 553). Springer Science & Business Media.

20. Croisier, F., & Jérôme, C. (2013). Chitosan-based biomaterials for tissue engineering. *European Polymer Journal*, *49*(4), 780-792.

21. Rabea, E. I., Badawy, M. E. T., Stevens, C. V., Smagghe, G., & Steurbaut, W. (2003). Chitosan as antimicrobial agent: applications and mode of action.*Biomacromolecules*, *4*(6), 1457-1465.

22. Jennings, J. A., & Bumgardner, J. D. (Eds.). (2016). *Chitosan Based Biomaterials Volume 2: Tissue Engineering and Therapeutics*. Woodhead Publishing.

23. Connell, L. S., Romer, F., Suárez, M., Valliant, E. M., Zhang, Z., Lee, P. D., & Jones, J. R. (2014). Chemical characterisation and fabrication of chitosan–silica hybrid scaffolds with 3-glycidoxypropyl trimethoxysilane. *Journal of Materials Chemistry B*, *2*(6), 668-680.

24. Tay, F. R., Durán, G., Paula, A. J., & Durán, N. (2015). Advances in Dental Materials through Nanotechnology: Facts, Perspectives and Toxicological Aspects.

25. Younes, I., Sellimi, S., Rinaudo, M., Jellouli, K., & Nasri, M. (2014). Influence of acetylation degree and molecular weight of homogeneous chitosans on antibacterial and antifungal activities. *International journal of food microbiology*,*185*, 57-63.

26. Bugnicourt, L., & Ladavière, C. (2016). Interests of chitosan nanoparticles ionically cross-linked with tripolyphosphate for biomedical applications. Progress in Polymer Science, 60, 1-

27. Raphel, J., Holodniy, M., Goodman, S. B., & Heilshorn, S. C. (2016). Multifunctional Coatings to Simultaneously Promote Osseointegration and Prevent Infection of Orthopaedic Implants. *Biomaterials*.

28. Ordikhani, F., Tamjid, E., & Simchi, A. (2014). Characterization and antibacterial performance of electrodeposited chitosan–vancomycin composite coatings for prevention of implant-associated infections. *Materials Science and Engineering: C*, *41*, 240-248.

29. Swanson, T. E., Cheng, X., & Friedrich, C. (2011). Development of chitosan–vancomycin antimicrobial coatings on titanium implants. *Journal of Biomedical Materials Research Part A*, *97*(2), 167-176.

30. Paladini, F., Pollini, M., Sannino, A., & Ambrosio, L. (2015). Metal-based antibacterial substrates for biomedical applications. *Biomacromolecules*, *16*(7), 1873-1885.

31. Budnyak, T. M., Pylypchuk, I. V., Tertykh, V. A., Yanovska, E. S., & Kolodynska, D. (2015). Synthesis and adsorption properties of chitosan-silica nanocomposite prepared by sol-gel method. Nanoscale research letters, 10(1), 87.

32. Spirk, S., Findenig, G., Doliska, A., Reichel, V. E., Swanson, N. L., Kargl, R., & Stana-Kleinschek, K. (2013). Chitosan–silane sol–gel hybrid thin films with controllable layer thickness and morphology. Carbohydrate polymers, 93(1), 285-290.

33. Juan-Díaz, M. J., Martínez-Ibáñez, M., Lara-Sáez, I., da Silva, S., Izquierdo, R., Gurruchaga, M., & Suay, J. (2016). Development of hybrid sol–gel coatings for the improvement of metallic biomaterials performance. *Progress in Organic Coatings*, *96*, 42-51.

34. Reiner, T., Kababya, S., & Gotman, I. (2008). Protein incorporation within Ti scaffold for bone ingrowth using Sol-gel SiO2 as a slow release carrier. *Journal of Materials Science: Materials in Medicine*, *19*(2), 583-589.

35. Gallardo, J., Galliano, P., & Duran, A. (2001). Bioactive and protective sol-gel coatings on metals for orthopaedic prostheses. *Journal of sol-gel science and technology*, *21*(1-2), 65-74.

36. Balgude, D., & Sabnis, A. (2012). Sol–gel derived hybrid coatings as an environment friendly surface treatment for corrosion protection of metals and their alloys. *Journal of sol-gel science and technology*, *64*(1), 124-134.

37. Trujillo, S., Pérez-Román, E., Kyritsis, A., Gómez Ribelles, J. L., & Pandis, C. (2015). Organic–inorganic bonding in chitosan–silica hybrid networks: physical properties. *Journal of Polymer Science Part B: Polymer Physics*, *53*(19), 1391-1400..

38. Shirosaki, Y., Tsuru, K., Hayakawa, S., Osaka, A., Lopes, M. A., Santos, J. D., & Fernandes, M. H. (2005). In vitro cytocompatibility of MG63 cells on chitosan-organosiloxane hybrid membranes. *Biomaterials*, *26*(5), 485-493.

39. Shirosaki, Y., Okayama, T., Tsuru, K., Hayakawa, S., & Osaka, A. (2008). Synthesis and cytocompatibility of porous chitosan–silicate hybrids for tissue engineering scaffold application. *Chemical Engineering Journal*, *137*(1), 122-128.

40. Lippmaa, E., Mägi, M., Samoson, A., Engelhardt, G., & Grimmer, A. R. (1980). Structural studies of silicates by solid-state high-resolution silicon-29 NMR. Journal of the American Chemical Society, 102(15), 4889-4893.

41. Davis, S. R., Brough, A. R., & Atkinson, A. (2003). Formation of silica/epoxy hybrid network polymers. *Journal of non-crystalline solids*, *315*(1), 197-205.

42. Wang, D., Romer, F., Connell, L., Walter, C., Saiz, E., Yue, S., & Jones, J. R. (2015). Highly flexible silica/chitosan hybrid scaffolds with oriented pores for tissue regeneration. *Journal of Materials Chemistry B*, *3*(38), 7560-7576.

43. Greenwood, P., & Gevert, B. (2011). Aqueous silane modified silica sols: theory and preparation. *Pigment & Resin Technology*, *40*(5), 275-284.

44. Hench, L. L., & Ethridge, E. C. (1972). Biomaterials: an interfacial approach.*Academic Press, Inc., 1972,*, 385.

45. Zolkov, C., Avnir, D., & Armon, R. (2004). Tissue-derived cell growth on hybrid sol–gel films. *Journal of Materials Chemistry*, *14*(14), 2200-2205.

46. Rupp, F., Gittens, R. A., Scheideler, L., Marmur, A., Boyan, B. D., Schwartz, Z., & Geis-Gerstorfer, J. (2014). A review on the wettability of dental implant surfaces I: theoretical and experimental aspects. *Acta biomaterialia*, *10*(7), 2894-2906.

47. Romero-Gavilán, F., Barros-Silva, S., García-Cañadas, J., Palla, B., Izquierdo, R., Gurruchaga, M., & Suay, J. (2016). Control of the degradation of silica sol-gel hybrid coatings for metal implants prepared by the triple combination of alkoxysilanes. *Journal of Non-Crystalline Solids*, *453*, 66-73.

48. Shirosaki, Y., Tsuru, K., Hayakawa, S., Nakamura, Y., Gibson, I. R., & Osaka, A. (2011). Effects of Si (IV) released from chitosan-silicate hybrids on proliferation and differentiation of MG63 osteoblast cells. *Bioceramics Development and Applications*, *1*.

49. Deligianni, D. D., Katsala, N. D., Koutsoukos, P. G., & Missirlis, Y. F. (2000). Effect of surface roughness of hydroxyapatite on human bone marrow cell adhesion, proliferation, differentiation and detachment strength. *Biomaterials*,*22*(1), 87-96.

50. Nishimoto, S. K., Nishimoto, M., Park, S. W., Lee, K. M., Kim, H. S., Koh, J. T., & Yang, Y. (2008). The effect of titanium surface roughening on protein absorption, cell attachment, and cell spreading. *International Journal of Oral & Maxillofacial Implants*, *23*(4).

51. Marinucci, L., Balloni, S., Becchetti, E., Belcastro, S., Guerra, M., Calvitti, M., & Locci, P. (2006). Effect of titanium surface roughness on human osteoblast proliferation and gene expression in vitro. *International Journal of Oral & Maxillofacial Implants*, *21*(5).

Table 1: Nomenclature of hybrid coatings formulated using the selected alkoxysilane mixtures and different amounts of chitosan.

NOMENCLATURE	%MTMOS	%GPTMS	%TEOS	%CHITOSAN
50M50G	**50**	**50**	**0**	0%
50M50G_2%				2%
50M50G_5%				5%
50M50G_10%				10%
45M45G10T	**45**	**45**	**10**	0%
45M45G10T_2%				2%
45M45G10T_5%				5%
45M45G10T_10%				10%

Table 2: Chemical shift values (δ) and the ratios of peak areas for 50M50G and 45M45G10T.

FORMULATION	**δ (ppm)** T_2, T_3	**Ratio of peak areas** T_2/T_3
50M50G	-59, -68	28/72
50M50G_2%		18/82
50M50G_5%		27/73
50M50G_10%		58/42
	δ (ppm) T_2, T_3, Q_3, Q_4	**Ratio of peak areas** $T_2/T_3/Q_3/Q_4$
45M45G10T	-59, -68, -102, -110	26/74/0/0
45M45G10T_2%		45/55/0/0
45M45G10T_5%		43/57/0/0
45M45G10T_10%		53/47/0/0

FIGURE CAPTIONS

Figure 1. Liquid-state ^{29}Si-NMR spectra of 50M50G and 50M50G_5% (a) and 45M45G10T and 45M45G10T_5% (b) hybrids

Figure 2. Solid-state ^{13}C-NMR of (a) 50M50G and (b) 50M50G_5%

Figure 3. Solid-state ^{29}Si-NMR spectra of (a) 50M50G and (b) 45M45G10T with and without chitosan

Figure 4: Contact angle values for the hybrid coatings

Figure 5. Mass loss due to hydrolytic degradation of 50M-50G and 45M-45G-10T coatings

Figure 6. Silicon release from the coatings versus time.

Figure 7: Cell viability for 50M-50G and 45M45G10T materials expressed as a percentage of viability in control samples.

Figure 8: Adhesion and proliferation of HFBs on 50M50G (a) and 45M45G10T coatings (b) and on titanium after 1, 3, 7 and 14 days of culture.

Figure 9: SEM images of the cell monolayer and cell agglomerates formed on the substrate surfaces.

Figure 10: Antibacterial activity of 50M50G (a) and 45M45G10T coatings (b).